Journal of Alloys and Compounds 506 (2010) 36–45

Contents lists available at ScienceDirect

Journal of Alloys and Compounds

journal homepage: www.elsevier.com/locate/jallcom

Magnetic properties of $TbFe_6Sn_6$ from neutron diffraction and ^{119}Sn Mössbauer spectroscopy

G. Venturini[a,*], B. Malaman[a], B. Ouladdiaf[b]

[a] Institut Jean Lamour, CNRS (UMR 7198), Nancy Université, B.P. 70239, 54506 Vandoeuvre-les-Nancy Cedex, France
[b] Institut Laue-Langevin, Boite Postale 156, 38042 Grenoble Cedex 9, France

ARTICLE INFO

Article history:
Received 6 May 2010
Received in revised form 17 June 2010
Accepted 23 June 2010
Available online 14 July 2010

Keywords:
Lanthanide alloys and compounds
Neutron diffraction
Mössbauer spectroscopy

ABSTRACT

A polycrystalline sample of $TbFe_6Sn_6$ has been studied by X-ray and neutron diffraction, magnetometric measurements and ^{119}Sn Mössbauer spectroscopy. The compound crystallizes in the orthorhombic Cmcm $TbFe_6Sn_6$-type. The iron sublattice orders at 554 K into an antiferromagnetic structure characterized by ferromagnetic (1 0 0) planes antiferromagnetically coupled, the moment being aligned along [1 0 0]. Below T_c = 27 K, the terbium sublattice orders ferromagnetically with the moments aligned along [1 0 0]. Simultaneously, the direction of the Fe moments tilts towards the (1 0 0) plane and a ferromagnetic canting opposite to the Tb moments takes place. At 2 K, the moments values are $\mu_{Tb} = 8.04(12)\,\mu_B$ and $\mu_{Fe} = 2.14(3)\,\mu_B$ and the canting angle is $\phi = 21(2)^\circ$. The ^{119}Sn Mössbauer spectroscopy has been performed in the 4.2–300 K range. Between the room temperature and T_c, only the tin site (Sn_5) experiences a transferred hyperfine field of about 22 T. Below T_c, all tin sites are concerned and the hyperfine field of Sn_5 decreases by ≈7 T, a feature attributed to a change of the anisotropic contribution to this hyperfine field. Attempts to correlate the hyperfine values to the characteristics of the structure are proposed.

1. Introduction

The magnetic properties of LFe_6X_6 compounds (L = Sc, Y, lanthanide; X = Ge, Sn) have been extensively studied by many different research groups [1–5]. The iron sublattice orders well above the room temperature into an antiferromagnetic structure consisting of ferromagnetic iron Kagomé planes antiferromagnetically coupled along the stacking direction. The lanthanide sublattice orders at low temperature into different magnetic arrangements and it has been assumed that the two sublattices were quite decoupled and that they ordered independently [6].

A recent study of the hexagonal $HfFe_6Ge_6$-type $TbFe_6Sn_4Ge_2$ pseudo-ternary compound has evidenced a new phenomenon [7]. In this simple crystal structure, stabilised by the partial replacement of tin by germanium, it has been observed unambiguously that the ordering of the terbium sublattice was accompanied by a slight bending of the iron antiferromagnetic collinear arrangement giving evidence of a non-negligible interaction between the two magnetic species.

In this compound, the Ge substituting atom is preferentially located on the 2(c) site of the $HfFe_6Ge_6$ structure, close to the terbium atoms lying in the 1(a) site, yielding strong shifts of the atomic positions and in turn a subsequent shortening of the Tb–Fe distances [8]. This feature might be invoked to explain the corresponding magnetic interaction and it has been decided to check this point by a neutron diffraction study of the parent ternary compound $TbFe_6Sn_6$ though this alloy orders into a rather more complicated but closely related orthorhombic structure [9].

The results of neutron experiment have shown that the ordering of the Tb sublattice was accompanied by a reorientation of the iron moments. This feature can provide information on the anisotropic contribution to the hyperfine field transferred at the ^{119}Sn nucleus as previously checked on LMn_6Sn_6 compounds (L = lanthanide) [10,11]. For this reason the neutron study has been completed by ^{119}Sn Mössbauer spectroscopy investigations.

2. Experimental methods

The sample has been prepared starting from the stoichiometric mixture of the elements, put into an alumina crucible, sealed in silica tube under argon and annealed for 5 days at 800 °C. After this preliminary chemical reaction, there is almost no remaining elemental tin and the resulting ingot can be finely ground to ensure homogeneity. The powder is then compacted in a pellet and put again at 800 °C for 2 weeks. After this second thermal treatment, X-ray diffraction analysis (Guinier Co $K\alpha_1$) reveals a well crystallized compound with, however, some remaining impurities lines indexed as the well known phases: $FeSn_2$, Sn, Tb_2O_3 and $TbFe_xSn_2$ [12].

To check the order and stoichiometry of the terbium atoms in the corresponding $TbFe_6Sn_6$-type structure, the intensities have been recorded on an XPert Pro powder diffractometer (Cu Kα) and the structure has been refined using the FULLPROF software [13].

* Corresponding author. Tel.: +33 3 83 68 46 73; fax: +33 3 83 68 46 11.
E-mail address: Gerard.Venturini@lcsm.uhp-nancy.fr (G. Venturini).

0925-8388/$ – see front matter © 2010 Elsevier B.V. All rights reserved.
doi:10.1016/j.jallcom.2010.06.208

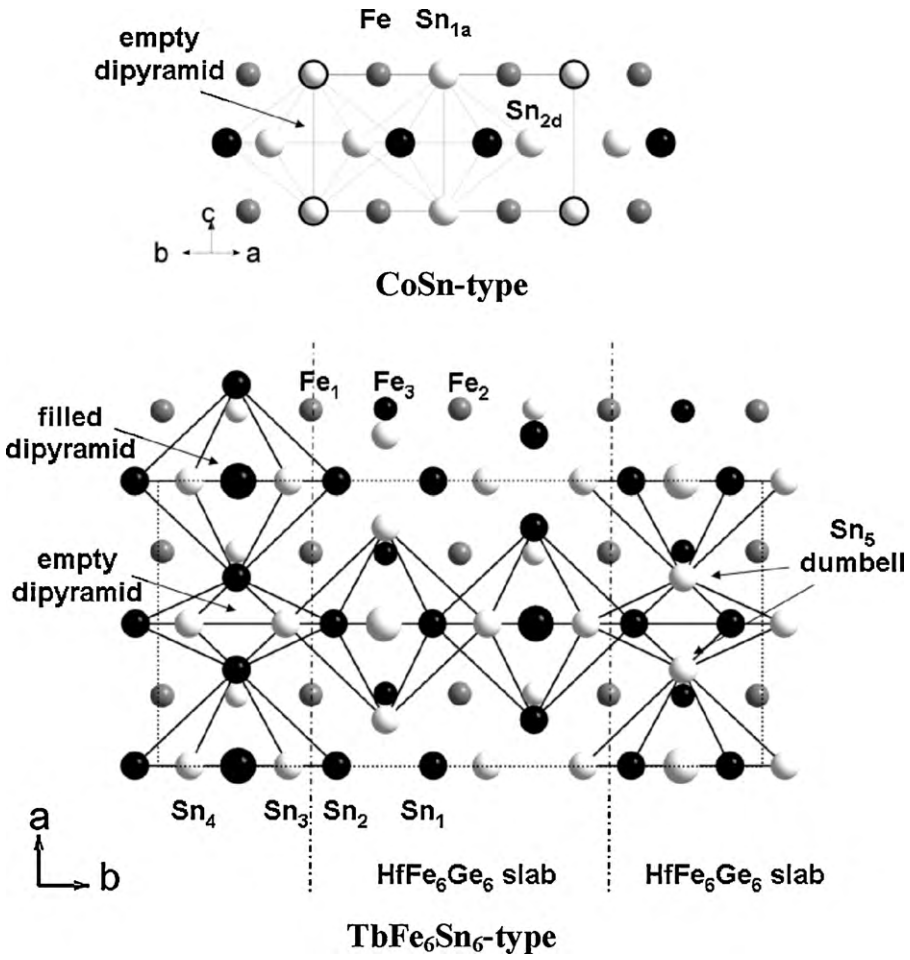

Fig. 1. Projection of the FeSn structure along [1 1 0] and $TbFe_6Sn_6$ structure along [0 0 1] (small circle = Fe, middle circle = Sn, large circle = Tb).

The neutron diffraction study has been performed on the D1b apparatus at the Institut Laue Langevin (Grenoble) and the magnetic structures have been refined using the FULLPROF software.

The ^{119}Sn Mössbauer measurements were carried out using a constant-acceleration spectrometer in standard transmission geometry. Several spectra were recorded between 300 and 4.2 K in a liquid helium cryostat. The velocity scale was calibrated with a ^{57}CoRh source (25 mCi) and a metallic iron foil at room temperature. We used a $Ba^{119m}SnO_3$ source (10 mCi) kept at room temperature which also served as the reference for the isomer shifts. A polycrystalline absorber with natural abundance of ^{119}Sn isotope and thickness of ~15 mg cm^{-2} was used. A palladium foil of 0.5 mm thickness was used as a critical absorber for tin X-rays. The Mössbauer spectra were fitted with a least-squares method program assuming Lorentzian peaks [14].

3. Results

3.1. Crystal structure refinement

The phase $TbFe_6Sn_6$ should be regarded as a filled derivative of a CoSn-type FeSn compound [15]. The Tb atoms occupy half of the empty hexagonal dipyramids of the CoSn-type in an ordered manner giving rise to an orthorhombic superstructure with cell parameters $a_o = 2 \cdot c_{CoSn}$; $b_o = 2 \cdot \sqrt{3}\, a_{CoSn}$; $c_o = a_{CoSn}$ (Fig. 1). Along the pseudo-hexagonal axis, the pyramids are alternately empty and filled by the Tb atoms. The insertion of Tb atoms in the host CoSn-type structure mainly acts on the Sn atoms building the apex of the dipyramids. These atoms are displaced towards the empty adjacent dipyramids giving rise to the formation of a Sn–Sn dumbbell. The Fe atoms and the remaining Sn atoms are almost unaffected by the insertion and the Fe Kagomé net remains unchanged.

The crystal structure of $TbFe_6Sn_6$ has been refined using the data from a single crystal study of the isotypic $DyFe_6Sn_6$ compound [16] as a starting point. A slight under-stoichiometry on the site of the lanthanide atom has been reported for several LFe_6Sn_6 compounds [5]. In order to check the occurrence of a similar phenomenon in the present compound, the occupancy factor (m_j) of the terbium site has been refined together with that of the Sn_5 site i.e. the tin atoms building the apex of the [$TbSn_8$] dipyramids (see Fig. 1). Correlatively, it has been assumed that the Sn_5 atoms, close to the Tb vacancies, moved towards a new Sn_5' site namely in its original position in the CoSn-type subcell (Sn_{1a} in Fig. 1). The three occupancy factors have been constrained by the relations: $2 \cdot m_{Tb} = m_{Sn_5} = (1 - m_{Sn_5'})$. The refinements lead to atomic positions close to those refined for $DyFe_6Sn_6$ and to a slight non-stoichiometry on the Tb site. The refined parameters are gathered in Table 1.

3.2. Magnetic measurements

The thermomagnetic measurements evidence a Néel point at 554 K and a Curie-like transition temperature at 27 K which should be related to the ordering of the terbium sublattice (Fig. 2). The magnetisation displays a linear behaviour at room temperature with a susceptibility of 55×10^{-6} emu/g (Fig. 3). The magnetisation measurements performed at 4.2 K show the behaviour of a hard magnetic material and the reversibility range is not reached in the maximum applied field (1.5 T) for which we observe a magnetisation of $M = 2.5(1)\,\mu_B$/mol. The curve in decreasing fields displays a large remanent magnetisation of $2.0(1)\,\mu_B$/mol. In order to get

Table 1
Atomic positions and occupancy factors of $TbFe_6Sn_6$ from X-ray data.

Sites	Wyckoff position	Point symmetry	x	y	z	m_j
Tb	4c	mm	0	0.128(1)	1/4	0.226(2)
Sn_5	8g	m	0.3407(4)	0.124(1)	1/4	0.452(3)
Sn_{5p}	8g	m	0.25	0.124(1)	1/4	0.048(3)
Sn_1	4c	mm	1/2	0.0384(3)	3/4	0.25
Sn_2	4c	mm	1/2	0.2034(3)	3/4	0.25
Sn_3	4c	mm	0	0.2051(3)	3/4	0.25
Sn_4	4c	mm	0	0.0411(3)	3/4	0.25
Fe_1	8d	$\bar{1}$	1/4	1/4	0	0.50
Fe_2	8e	2	0.248(1)	0	1/2	0.50
Fe_3	8g	m	0.245(1)	0.132(1)	3/4	0.50

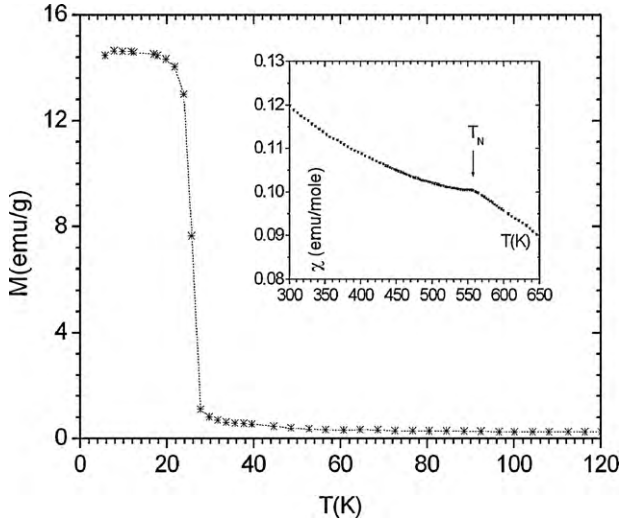

Fig. 2. Low temperature thermal variation of the magnetisation of a $TbFe_6Sn_6$ free sample under an applied field of 0.1 T (insert shows the variation of the susceptibility above the room temperature).

a suitable value of the saturation magnetisation, we have performed a free-powder experiment. One obtains a maximum value ($M = 3.7(2)\,\mu_B$/mol) larger than the value measured on the fixed sample (Fig. 3) but still significantly smaller than the Tb free ion

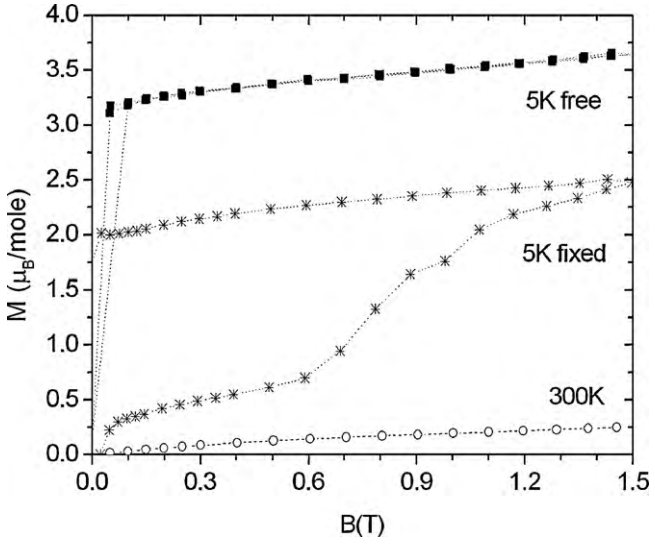

Fig. 3. Isotherm magnetisation curves of $TbFe_6Sn_6$ at 300 and 5 K (fixed and free sample).

value ($9\,\mu_B$) thus suggesting a ferrimagnetic arrangement between the Tb and Fe sublattices.

3.3. Neutron diffraction

3.3.1. High temperature magnetic structure (T = 50 K)

A long duration neutron diffraction pattern has been recorded at 50 K, namely well above the ordering point of the Tb sublattice (Fig. 4). This pattern is mainly characterized by the occurrence of several magnetic lines obeying the rule ($h + k = 2n + 1$) namely an anti-C mode. The only lines displaying significant intensities are the pairs (1 2 1)//(1 4 0), (1 0 2)//(1 6 1), (1 4 2)//(1 8 0) (Fig. 4) which obviously correspond to the $(10½)_H$, $(11½)_H$ and $(20½)_H$ lines of the CoSn-type hexagonal subcell. This means that the magnetic ordering of the iron sublattice keeps the pseudo-hexagonal symmetry and in turn that the Fe Kagomé planes are ferromagnetic. The absence of additional magnetic lines corresponding to the orthorhombic symmetry does not allow us to refine individual moment magnitude for the three iron sites and a common iron moment has been considered. The Kagomé planes are antiferromagnetically coupled each to the others along the [0 0 1] direction of the hexagonal subcell i.e. along the [1 0 0] direction of the Cmcm $TbFe_6Sn_6$-type cell (Fig. 5). This kind of ordering is classically observed in all the known $HfFe_6Ge_6$-type RFe_6X_6 compounds as well as in the already studied compounds RFe_6X_6 crystallizing in the orthorhombic variants [4–7,17–19]. The absence of the (1 0 0) line indicates that the Fe moments are aligned along [1 0 0], namely along the sixfold axis of the hexagonal subcell. The moment magnitude has been refined to the final value $\mu_{Fe} = 2.41(4)\,\mu_B$ ($R_{magn} = 5.15\%$). The refined parameters are gathered in Table 2 and the observed and calculated patterns are displayed in Fig. 4.

3.3.2. Low temperature magnetic structure (T = 2 K)

The low temperature magnetic transition is accompanied by several characteristic changes in the neutron diffraction pattern. Regarding the anti-C lines, one observed a decrease of the inten-

Table 2
Refined magnetic parameters of $TbFe_6Sn_6$ at 50 and 2 K.

	50 K	2 K
a (Å)	8.916(2)	8.921(1)
b (Å)	18.61(1)	18.635(7)
c (Å)	5.396(2)	5.386(2)
f_{cor}	0.02(1)	0.020(9)
μ_{Fe_AF} (μ_B)	2.41(4)	2.14(4)
μ_{Fe_F} (μ_B)	–	0.66(7)
μ_{Fe_Total} (μ_B)	2.41(4)	2.24(5)
θ (°)	90	90
ϕ (°)	0	73(2)
μ_{Tb} (μ_B)	0	8.7(2)
R_{Bragg}; R_f; R_{magn}	3.25; 4.40; 5.15	2.46; 2.11; 5.36
R_{wp}; R_{exp}; χ^2	7.19; 2.51; 8.22	7.70; 1.33; 33.6

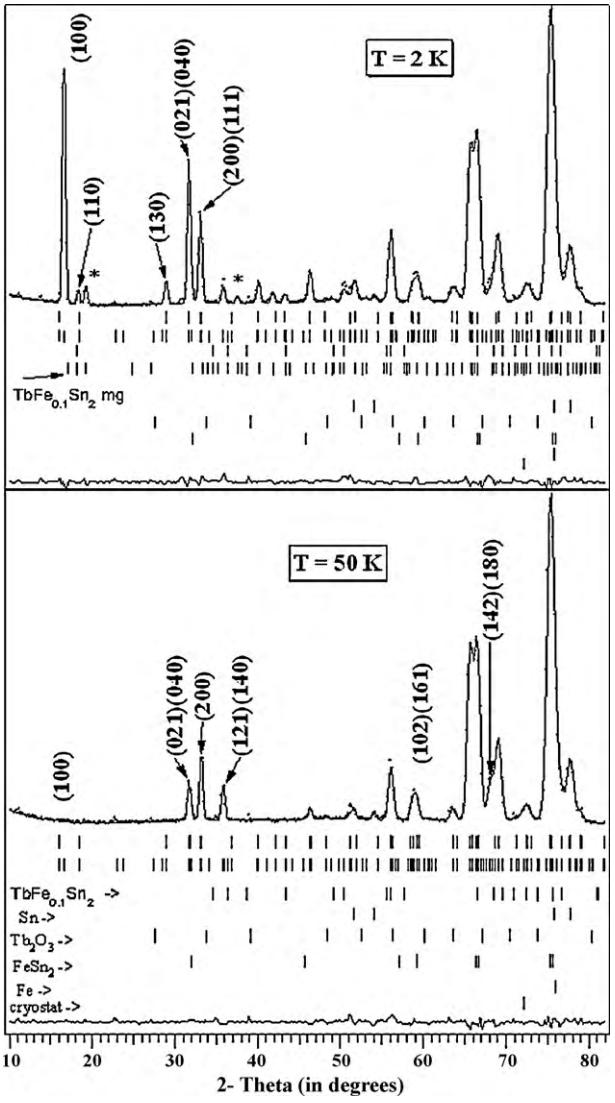

Fig. 4. Observed and calculated neutron patterns of $TbFe_6Sn_6$ at 50 and 2 K (* indicates the magnetic lines of $TbFe_xSn_2$ impurity [12]).

sity of the (1 2 1)//(1 4 0) pair and the apparition of the (1 0 0) line (Figs. 4 and 6). This evolution may be interpreted as a spin-reorientation of the iron moments from the [1 0 0] direction toward the (1 0 0) plane. Regarding the C-centred lines, one observed a large increase of the intensities of the (0 2 1)//(0 4 0) pair, which previously exhibited a pure nuclear contribution, and the apparition of the (1 1 0) and (1 3 0) lines whose nuclear contributions are nearly zero. Regarding the (2 0 0) line intensity, it displays only a slight increase which should be mainly attributed to the growth of the (1 1 1) companion, therefore suggesting that the terbium moments are aligned along the [1 0 0] direction. The following constraints have been taken into account in the preliminary refinements: antiferromagnetic Fe sublattice with the moments aligned along [0 1 0] and ferromagnetic Tb sublattice with the moments aligned along [1 0 0]. This leads to a rather good reliability between the observed and calculated intensities (R_{magn} = 9.41%). However, at this step, a few lines display weak discrepancies and the amplitude of the Tb moment (μ_{Tb} = 8.04 μ_B) yields a net magnetisation strongly larger than that deduced from the macroscopic magnetic measurements at 5 K (3.7(3) μ_B).

In order to reduce the net magnetisation and to improve the fit of the diffracted intensities, a small ferromagnetic component, opposite to the Tb moment, has been introduced on the Fe sublattice by bending the Fe moments lying in the $x \approx 0.25$ and 0.75 (1 0 0) planes with the same angle. This action improves the reliability factor (R_{magn} = 5.36%) giving rise to a ferromagnetic component on the Fe sublattice of μ_{Fe} = 0.66(7) μ_B) opposite to the direction of the Tb moment (μ_{Tb} = 8.7(2) μ_B). The resulting calculated magnetisation is now M = 4.74 μ_B/mol, closer to the experimental value (3.7(3) μ_B/mol). The value of the antiferromagnetic component of the Fe moment ($\mu_{AF.Fe}$ = 2.14(4) μ_B), aligned along [0 1 0], gives rise to a total Fe moment μ_{Fe} = 2.24(5) μ_B and a bending angle α = 17(2)° (Fig. 5).

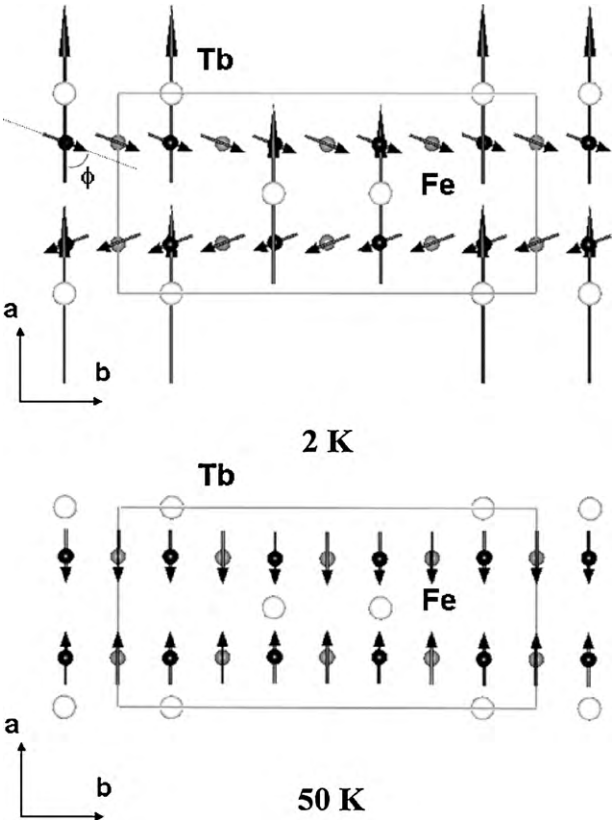

Fig. 5. Projection along [0 0 1] of the magnetic structures of $TbFe_6Sn_6$ at 50 and 2 K.

Remark: Attempt to align the antiferromagnetic component along the [0 0 1] direction does not significantly change the residual factor. This feature should be related to the pseudo-hexagonal

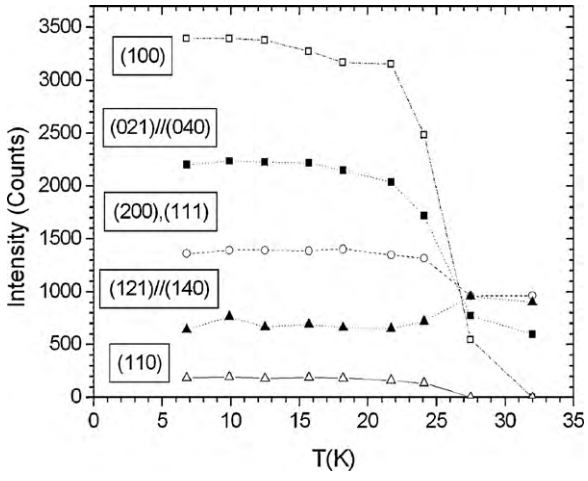

Fig. 6. Variation of the intensity of some characteristic diffraction peaks of $TbFe_6Sn_6$.

symmetry of this compound: any change in the orientation of the Fe moment in the (1 0 0) plane will lead to different ratio in the intensities of the lines belonging to the pseudo-hexagonal pairs. Such differences cannot be checked from powder diffraction experiments.

3.4. Discussion

The compound $TbFe_6Sn_6$ displays a particular magnetic behaviour never observed in other LT_6X_6 compounds. At 27K, the ordering of the Tb sublattice yields an abrupt spin-reorientation of the Fe moments from the pseudo-hexagonal axis towards the (1 0 0) plane. Furthermore, this transition goes with the appearance of an additional antiferromagnetic interaction between the two sublattices yielding a small canting on the iron moments. Assuming a strong uniaxial anisotropy of the Tb moments, the energy of this magnetic structure may be written in a simplified expression

$$E = J_{Fe-Fe} \cos 2\phi - J_{Tb-Fe} \cos \phi + K_{Fe} \sin^2 \phi \quad (1)$$

where J_{Fe-Fe} is the interplane Fe–Fe interaction, J_{Tb-Fe} the interaction between the Fe and Tb sublattices, K_{Fe} the anisotropy constant of the Fe moment and ϕ the canting angle as defined in Fig. 7a. The ϕ value giving rise to a stable configuration is given by $\partial E/\partial\phi = 0$ leading to the following expression:

$$\cos \phi = J_{Tb-Fe}/(4J_{Fe-Fe} - 2K_{Fe}) \quad (2)$$

According to the neutron diffraction, $\phi = 73^\circ$, giving: $J_{Tb-Fe} = 0.292(4J_{Fe-Fe} - 2K_{Fe})$.

The relative energies of the canted, independent ordering and ferrimagnetic structures are depicted in Fig. 7. It shows that the stabilisation of the canted structure needs a K_{Fe}/J_{Fe-Fe} ratio smaller than 0.1 and for a given K_{Fe}/J_{Fe-Fe} ratio, a sufficiently large J_{Tb-Fe}/J_{Fe-Fe} ratio.

The compound $TbFe_6Sn_6$ being slightly understoichiometric, we guess that small change in the Tb vacancy concentration, via its play on the J_{Tb-Fe} quantity, might lead to different magnetic properties. The magnetic behaviour of $TbFe_6Sn_6$ is quite different to that of $TbFe_6Ge_6$ within which the Fe moments remain aligned along the pseudo-hexagonal axis [4] while a canting of the Fe sublattice has been previously observed in $TbFe_6Sn_4Ge_2$ [7]. In this latter case, this phenomenon is favoured by the axial anisotropy of the Fe moment and the in-plane anisotropy of the Tb moment.

The independent ordering of the Fe and L sublattices, previously described for $HoFe_6Sn_6$ and $ErFe_6Sn_6$ [19,20], probably arises from a J_{L-Fe} exchange interaction smaller than that observed in the present $TbFe_6Sn_6$ compound.

3.5. ^{119}Sn Mössbauer spectroscopy

In the orthorhombic $TbFe_6Sn_6$ structure, there are five inequivalent Sn atoms: four, labelled from 1 to 4, at 4c positions and one, labelled 5 in 8g position. As illustrated in Fig. 8, the Sn-4c atoms are located in similar slightly distorted trigonal prisms of Fe atoms with Fe–Sn distances ranging from 2.58 to 2.86 Å. Their coordinations are completed by the occurrence of 0, 1, 2, or 3 Tb atoms lying in the (1 0 0) planes at $x = 0$ or 1/2 (Fig. 8). The situation is quite different for the Sn_5 atom which lies in a position close to one Fe Kagomé plane (Fig. 8).

Above $T_t = 27$K, according to the magnetic structure, the four Sn_1 to Sn_4 sites, lying in mirror located between two antiferromagnetically coupled ferromagnetic iron planes, do not experience any transferred hyperfine field (Fig. 8a) whereas the Sn_5 site, which is near a ferromagnetic Fe plane, does experience a large hyperfine field.

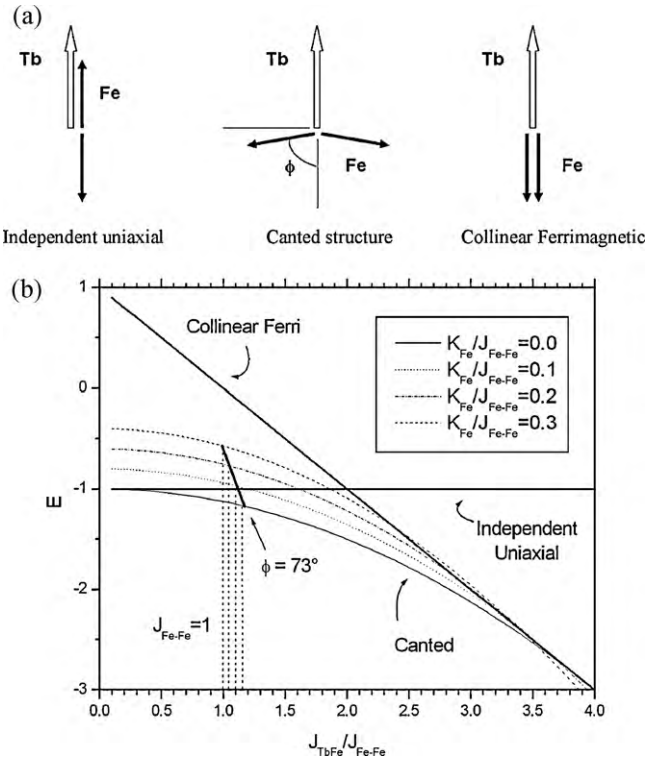

Fig. 7. (a) Several possible simple moment arrangements and (b) their relative stabilities.

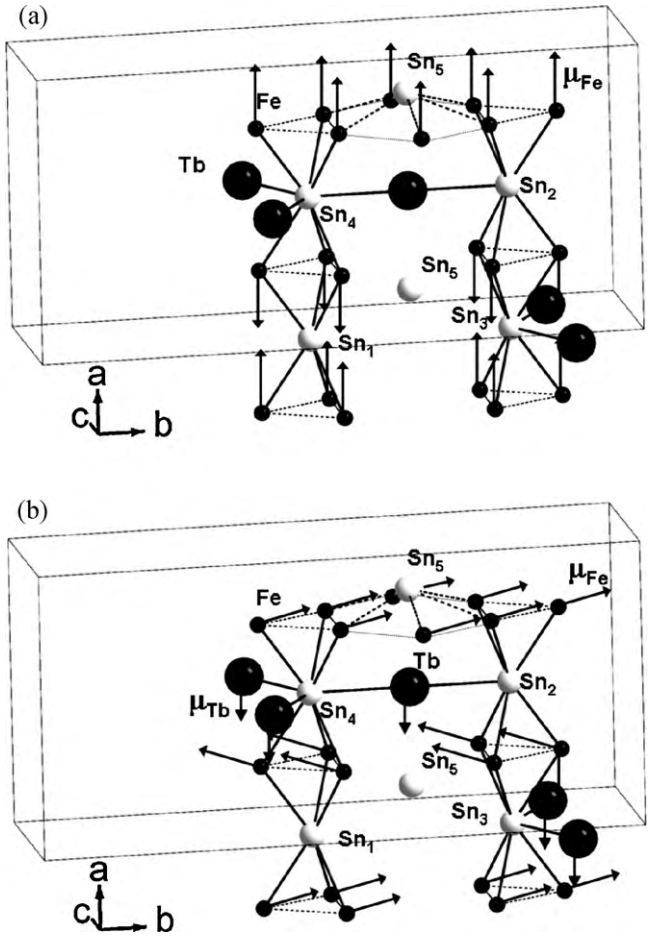

Fig. 8. Environment of the various Sn sites in the high and low temperature magnetic structures.

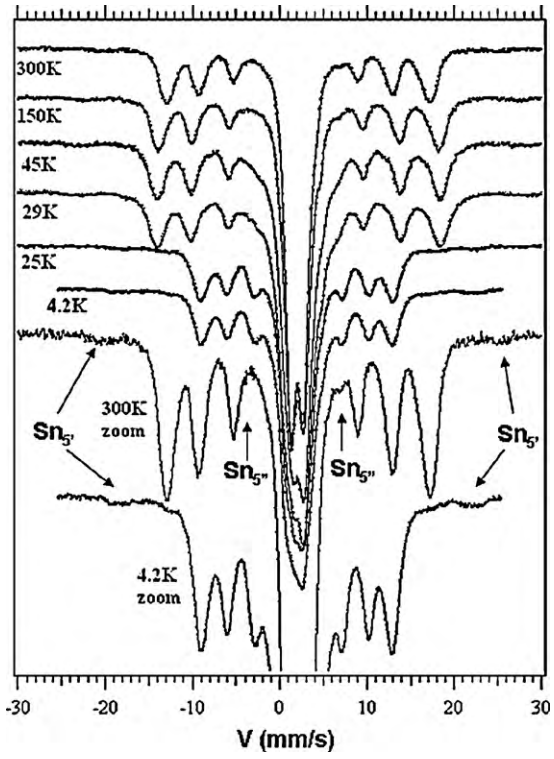

Fig. 9. Observed ^{119}Sn spectra at various temperatures (a zoom of the 300 and 4.2 K spectra is done to enhance the Sn_5' and Sn_5'' peaks).

At 2 K, due to the canted Fe sublattice and the ordering of the Tb sublattice, all the tin nuclei will experience more or less large hyperfine fields (Fig. 8b).

3.5.1. Description of the spectra

The spectrum recorded at 300 K is shown in Figs. 9 and 10. One observes a broadened and asymmetric doublet which can be attributed to the sum of the doublets corresponding to the Sn_1, Sn_2, Sn_3 and Sn_4 sites. Secondly, one observes a sextet characteristic of tin nuclei experiencing large hyperfine fields (≈20 T) which should be attributed to the Sn_5 site. It is worth noting that the peaks of this sextet are relatively broadened and display asymmetrical shapes.

Moreover, a very careful examination of the spectrum (Fig. 9) evidences the occurrence of very weak external peaks which should be attributed to the V1 and V6 components of a sextet with a field greater than 30 T. Since its thermal field variation mirrors that of the

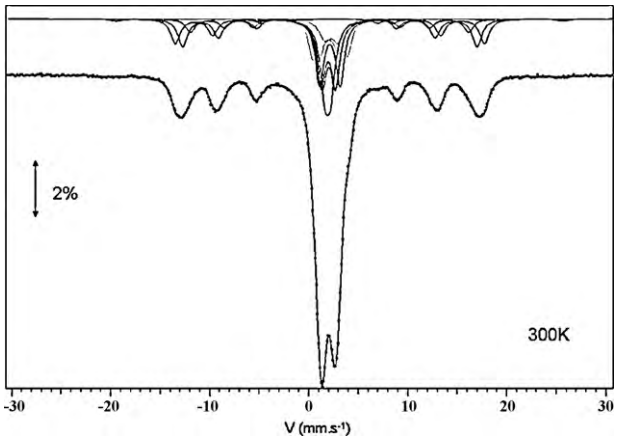

Fig. 10. Observed and calculated ^{119}Sn spectra of $TbFe_6Sn_6$ at 300 K.

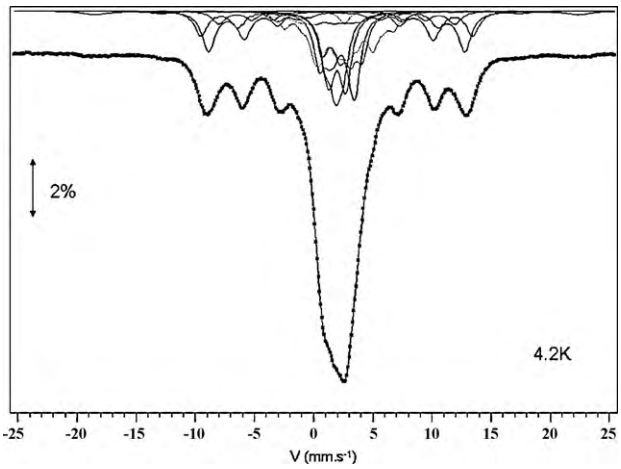

Fig. 11. Observed and calculated ^{119}Sn spectra of $TbFe_6Sn_6$ at 4.2 K.

previous sextet (see below), we guess that this sextet is intrinsic to $TbFe_6Sn_6$ as a Sn_5 sub-site. There is in addition a weak peak around +7 mm s^{-1} which should be attributed to a supplementary sextet with a rather weak field (≈0.9 T).

Finally, a minor part of the resonant area is ascribed to the $FeSn_2$ (*corresponding to the shoulder on the right side of the central doublet at* ≈+5 mm s^{-1}, Fig. 10) [22] and $TbSn_2$ impurities.

The spectrum recorded at 4.2 K displays a similar appearance (Figs. 9 and 11) but, this time, the central doublet presents a broadening which should be attributed to the magnetic splitting of the sites Sn_1, Sn_2, Sn_3 and Sn_4 associated to the (re)ordering of the (Fe) and Tb sublattices. Furthermore, the hyperfine fields corresponding to the Sn_5 sites have strongly decreased. As shown in Fig. 9, this phenomenon occurs abruptly at 27 K.

3.5.2. Fitting procedure and site attributions

Fits of the paramagnetic components of the spectrum yield $|\Delta_p|$ values where the total quadrupole splitting Δ_p is given by:

$$\Delta_p = \frac{eQV_{ZZ}}{2}\sqrt{\left(1+\frac{\eta^2}{3}\right)}$$

High H_{hf} values imply to consider the quadrupole interaction as a perturbation of the magnetic hyperfine interaction (first order approximation). The fits thus allow extracting the apparent quadrupolar (2ε) splitting which is related to the quadrupolar interaction $\Delta = eQV_{zz}/2$ by:

$$2\varepsilon = \Delta\left[\frac{3\ \cos^2\theta - 1 + \eta\ \sin^2\theta\ \cos 2\varphi}{2}\right] \quad (3)$$

In this equation, θ and φ are, respectively, the polar and azimutal angles of the hyperfine field direction with respect to the electric field gradient (EFG) frame of reference. To know the orientation of the principal axes of the EFG tensor is not trivial in such orthorhombic structure. Nevertheless, from the analysis of Gaczynski et al. [21] for $DyFe_6Sn_6$, we have considered that V_{zz} is aligned along the pseudo-hexagonal axis [1 0 0] with an asymmetry parameter $\eta = 0$.

Otherwise, the Mössbauer spectra are fitted with a least-squares method program using the full Hamiltonian. The fits thus allow extracting the field H, the quadrupole splitting Δ, the isomer shift δ, the asymmetry parameter η and the angles θ and φ. It is however known that only H, δ and $|\Delta(1+\eta^2/3)^{1/2}|$ are determinated without ambiguity from such powder Mössbauer spectra. Once the optimal solution has been obtained, the Karyagin method [23] is then applied to the fitted energy levels. This fitting method finally gives: H, δ and $|\Delta(1+\eta^2/3)^{1/2}|$ and one or two ranges (Δ', Δ''), (θ', θ''), (η',

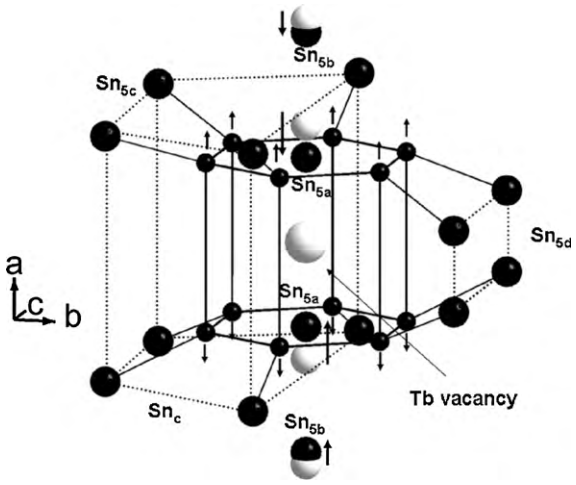

Fig. 12. Environment of the Tb vacancy (large white circle). The arrows indicate the possible atomic displacements of Fe and Sn atoms. For Sn_{5a} and Sn_{5b}, the white and black circles indicate the initial and possible final position. The Sn_{5c} and Sn_{5d} sites belonging to the same $HfFe_6Ge_6$ slab are linked by dotted lines.

η''), and (φ', φ'') for each site. In general, (θ', θ'') is of the order of a few degrees while wide intervals are obtained for η and φ.

The central component of the spectra has been attributed to the Sn_1, Sn_2, Sn_3 and Sn_4 sites and we have tried to fit individually their hyperfine parameters in order to examine the influence of their different Tb environments (Fig. 8). We are aware that the corresponding absorption peaks are strongly convoluted and that the results could be relatively inaccurate.

At 300 K, we have used four quadrupole doublets of equal intensity and linewidths (Γ_{FWHM}). At low temperature, these sites should experience a hyperfine field arising for the geometrical sum of the fields transferred from the Tb moment and from the ferromagnetic component of the Fe sublattice. According to the magnetic structure, these contributions are parallel to the [1 0 0] direction, i.e. $\theta = 0^\circ$. In this case, four sextets have been refined.

The external sextets and the additional weak peak (see above) have been attributed to the Sn_5 site and/or to the corresponding Sn_{5i} sub-sites. The subdivision of this site in several sub-sites arises from the under-stoichiometry in terbium. The Sn_5 site building the apex of the dipyramid centred by the Tb atom (or vacancy), we propose the following subdivision (Fig. 12):

- Sn_{5a} is the atom building the apex of a vacant dipyramid. It will probably move towards the vacancy and find a position close to that of Sn_{1a} in FeSn (Fig. 1). Its relative area will be proportional to the concentration of Tb vacancies.
- Sn_{5b} is the atom building the dumbbell with Sn_{5a}. Thus, the displacement of Sn_{5a} modifies the hyperfine parameters of Sn_{5b}. Its relative area will be also proportional to the concentration of vacancies.

These two sites have been attributed to the weak external peaks and to the weak internal peak at ≈+7 mm s^{-1}.

The widening of the main sextet has been attributed to tin atoms having a Tb vacancy as next nearest neighbour hereafter labelled Sn_{5c} and Sn_{5d} atoms (Fig. 12). This kind of Sn atoms having six Tb atoms as next nearest neighbour, their relative population (P_p) is significant and given by the binomial distribution:

$$P_p = C_p^6 \cdot x^p \cdot (1-x)^{6-p}$$

where p is the number of Tb vacancies and x is the concentration in Tb vacancies.

The change of their hyperfine parameters might arise from a displacement of the iron atoms around the vacancy. In the LT_6X_6 compounds, it is frequently observed that the transition metal planes are tightened around the L plane, a feature which has been interpreted as resulting from a significant L–T hybridization [24]. On the contrary, around the Tb vacancy, the Fe_{12} hexagonal prism might be inflated, a feature which will be experienced by the surrounding Sn atoms (see Fig. 12). According to the crystal structure of $TbFe_6Sn_6$, the 12 Sn atoms surrounding the Fe_{12} prism can be divided into 2 groups: 8 Sn atoms belonging to the same $HfFe_6Ge_6$ slab and 4 Sn atoms belonging to the adjacent $HfFe_6Ge_6$ slab (Figs. 1 and 12). According to this, a shortening of 8 Fe–Sn distances and a lengthening of 4 Fe–Sn distances are expected yielding a Sn_{5c} site twice populated as the Sn_{5d} site. This particularity explains the asymmetrical shape of the peaks of the main sextet (3 convoluted sextets).

For the weak external sextet and the main sextet, the high H_{hf} values imply to consider the quadrupole interaction as a perturbation. In the refinements, we have only constrained the linewidths (Γ) of the different components of the main sextet to be equal.

The site corresponding to the weak internal peak should be considered separately. The expected relatively low value of the field indicates that the quadrupole interaction cannot be considered as a perturbation. However, above 27 K, the neutron diffraction indicates that the moment are aligned along [1 0 0] giving rise to $\theta = 0^\circ$. In this case, a sextet has been refined. At low temperature, the hyperfine field arises from the geometrical sum of the contribution of the Tb moment aligned along [1 0 0] and of the Fe moment at 69° from this direction. Therefore, the internal weak site has been refined as an octuplet with the full Hamiltonian method in the low temperature range.

3.5.3. Results and comments

In all cases, the fitted isomer shifts (δ) range between 1.73 and 2.53 mm s^{-1}, typical values for such metallic compounds.

The spectrum recorded at 300 K (Fig. 10) has been fitted down to $\chi^2 = 2.07$ and the corresponding parameters are gathered in Table 3. The apparent quadrupole splittings (2ε) and isomer shifts (IS) values of the Sn_5, Sn_{5c} and Sn_{5d} sites are rather homogeneous in accordance with their similar environments. The fit indicates that the relative area of the site with the largest field (Sn_{5c}) is almost twice the area of the site with the smallest field (Sn_{5d}). This fea-

Table 3
^{119}Sn hyperfine parameters of $TbFe_6Sn_6$ at 300K ($\chi^2 = 2.07$).

Sites	P_i±0.03	Γ (mm s^{-1})±0.06	IS (mm s^{-1})±0.08	Δ_p (mm s^{-1})±0.08	2ε (mm s^{-1})±0.08	B_{hf} (T)±0.3
Sn_2	0.16	1.07	2.00	2.13	–	0
Sn_4	0.16	1.07	1.99	1.40	–	0
Sn_3	0.16	1.07	1.97	1.35	–	0
Sn_1	0.16	1.07	1.92	0.60	–	0
Sn_{5c}	0.13	1.14	1.98	–	0.33	22.8
Sn_5	0.14	1.14	1.99	–	0.31	21.7
Sn_{5d}	0.07	1.14	1.97	–	0.26	20.5
Sn_5'	0.01	1.51	2.03	–	0.63	33.4
Sn_5''	0.01	1.01	1.84	–	−1.92	8.8

Table 4
^{119}Sn hyperfine interaction parameters of $TbFe_6Sn_6$ at 4.2 K ($\chi^2 = 3.63$).

Sites	P_i±0.030	Γ (mm s^{-1})±0.06	IS (mm s^{-1})± 0.08	2ε (mm s^{-1})± 0.08	B_{hf} (T)± 0.3
Sn_2	0.146	1.12	2.45	1.90	1.0
Sn_4	0.146	1.12	2.18	1.44	0.2
Sn_3	0.146	1.12	2.16	1.54	0.9
Sn_1	0.146	1.12	1.74	0.47	2.0
Sn_{5c}	0.126	1.30	2.02	−0.12	16.7
Sn_5	0.169	1.30	2.03	−0.16	15.7
Sn_{5d}	0.049	1.30	2.00	−0.10	14.4
Sn_5'	0.029	2.46	2.08	−0.29	29.8
Sn_5''	0.044	1.30	2.18	−1.86	7.1

Range	Δ; Δ'	η; η'	θ; θ'	ϕ; ϕ'
Range of values for Sn_5''				
1	−1.85; −1.60	0; 1.0	58; 60°	0; 43°

ture is in good accordance with the site attributions proposed in the previous section. Therefore, it is suggested that the site with the intermediate field corresponds to the "pure" site Sn_5 namely without next nearest neighbour Tb vacancy.

The Sn_1, Sn_2, Sn_3 and Sn_4 sites are characterized by a rather wide range of Δ_p values. It is interesting to note that the averaged Δ values of the two largest (Sn_2 and Sn_4) and of the two smallest (Sn_1 and Sn_3) QS values (1.77 and 0.98 mm s^{-1} respectively) are very close to those measured in the isotypic $DyFe_6Sn_6$ compound, refined in the hexagonal approximation (1.81 and 1.00 mm s^{-1}) [21]. Therefore, the relatively wide range of Δ values observed for these compounds might be characteristic of the orthorhombic $TbFe_6Sn_6$ structural type.

For the two remaining weakly populated sites Sn_5' and Sn_5'', we can make the following remarks:

- both the Sn_5' and Sn_5'' sites are characterized by similar weak relative area (1%),
- the site Sn_5' is characterized by a strong hyperfine field (33 T),
- the site Sn_5'' is characterized by a strong negative 2ε value.

The spectrum recorded at 4.2 K (Fig. 11) has been fitted down to $\chi^2 = 2.90$ and the corresponding parameters are gathered in Table 4. The (2ε) values of the Sn_5, Sn_{5c}, Sn_{5d} and Sn_5' sites are still homogeneous but have changed by a factor close to −1/2 with respect to the 300 K values. According to Eq. (3) and the assumption of a V_{zz} direction parallel to [1 0 0], this result is in concordance with the Fe spins reorientation observed by neutron diffraction. Eq. (3) yields $\theta = 90°$ with $\eta = 0$, and in turn a rotation of the hyperfine fields from the [1 0 0] direction towards the [1 0 0] plane.

The hyperfine parameters of Sn_5'' do not drastically change from 300 to 4.2 K, except for the θ angle value which increases from 0 to 59° in relation with the reorientation and the canting of the iron moments: at 4.2 K, the field transferred from the close Fe plane makes an angle $\theta = 73°$ with the [1 0 0] direction and should be geometrically added to the field arising from the Tb sublattice aligned along [1 0 0] and, eventually, to the field arising from the next nearest neighbour Fe plane.

At 4.2 K, the Sn_1, Sn_2, Sn_3 and Sn_4 sites are still characterized by a rather wide range of Δ values similar to those refined in the non-magnetic state, in good accordance with the hexagonal setting which has been used for the analysis.

3.5.4. Discussion

In relation with severely convoluted multiplets, some results of this ^{119}Sn Mössbauer study must be considered carefully. However, the observed trends might provide several interesting information.

A first point deals with the proposed relations between the under-stoichiometry in terbium and the observed Sn_5 sub-sites.

The population of the Sn_a and Sn_b sites is directly related to the concentration of Tb vacancy (one Tb nearest neighbour). At 4.2 K, the refined populations, P_5' and P_5'', (Table 4) divided by the sum of the total Sn_5 site population ($P_T = 0.42$) lead to vacancy concentrations $C_{5a} = 0.069$ and $C_{5b} = 0.107$. The concentrations deduced from the other splitting P_{5c} and P_{5d} are related according to the binomial distribution:

$$P_p = C_p^6 \cdot x^p \cdot (1-x)^{6-p}$$

where 6 is the total Tb next nearest neighbours, p is the number of Tb vacancies and x the concentration in Tb vacancy. For 6 occupied sites ($p = 0$), $P_6 = (1-x)^6$ and for 1 vacant site ($p = 1$), $P_5 = 6x(1-x)^5$. Neglecting the next terms ($p = 2$ to 6), we can estimate x from the population P_5 of the Sn atoms having one Tb vacancy as next nearest neighbour (namely $P_{5cd} = P_{5c} + P_{5d}$) and the population $P_6 = P_T - P_{5cd}$. The resolution of the system gives $x = 0.128$.

The rather good reliability between the vacancy concentration deduced from Mössbauer spectroscopy and the value refined from X-ray data ($x_{XRD} = 0.096(4)$) agrees with the proposed starting hypothesis concerning the relation between the observed sub-sites and the presence of Tb vacancies.

The attribution of sites (Sn_5', Sn_5'') to atoms (Sn_{5a}, Sn_{5b}) is more intricate. Considering that the amplitude of the hyperfine field in only related to the spacing between the magnetic moments and the ^{119}Sn probe, it would be very tempting to attribute the Sn_{5a} atom moving towards the ferromagnetic plane to the Sn_5' site characterized by the largest H_{hf} value. On another hand, a possible relaxation of atom Sn_{5b} and the concomitant displacement away from the ferromagnetic plane might account for a reduction of the hyperfine field of Sn_5''. However, such hypothesis strongly disagrees with the Δ values of the Sn_5' and Sn_5'' sites. The Δ value of site Sn_5'' is very different to the Δ value of the remaining Sn_5 sites and more consistent with the Δ value of Sn_{1a} in FeSn and Sn_{2e3} in $U_{0.4}Fe_6Sn_6$ and $U_{0.6}Fe_6Sn_6$ ($\Delta = -2.90$ mm s^{-1}) [20]. On another hand, the Δ value of the site Sn_5' is more consistent with the Δ value of the remaining Sn_5 sites, a feature accounting for environments which are not very different. With such a distribution based on Δ values, it would be necessary to invoke a more complicated mechanism of field transfer to understand the corresponding field values.

An other interesting result from which trends may be proposed is the value of the transferred hyperfine fields on the Sn_1, Sn_2, Sn_3 and Sn_4 sites. At low temperature, the ferromagnetic canting of the iron sublattice yields a field transfer on the corresponding nuclei. Since there is also a field transfer arising from the terbium sublattice, we expect a geometric sum of both contributions. By analogy with the $HfFe_6Ge_6$ compounds [7], we guess that the site with the largest Δ value corresponds to the site 2d without Tb nearest neighbour. This site should mainly

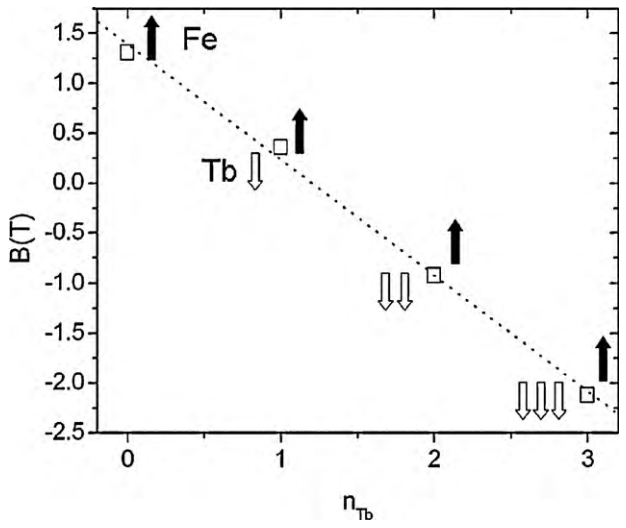

Fig. 13. Variation of the hyperfine field of the Sn_1, Sn_2, Sn_3 and Sn_4 sites as a function of the number of Tb neighbours.

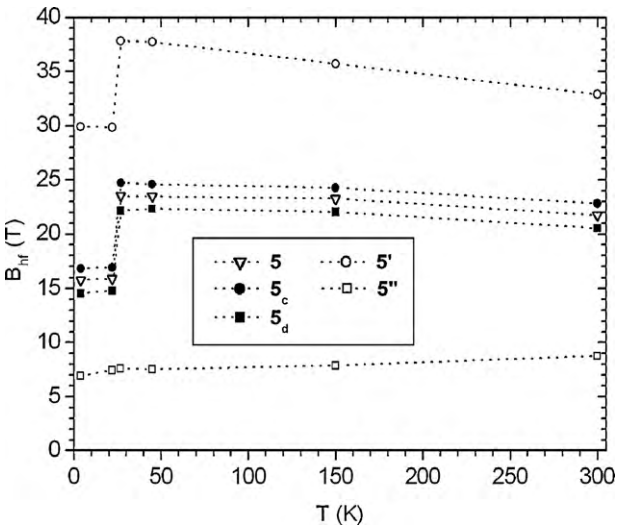

Fig. 14. Thermal variation of the hyperfine fields of Sn_5 sub-sites.

experience a hyperfine field transferred from the Fe environment (B_{hf} = 1.02 T). The other sites should experience a negative contribution increasing with the number of Tb close neighbours (Fig. 8). The best way to correlate the observed fields with the number of Tb neighbours is depicted in Fig. 13. A linear analysis of the field variation as a function of the number of Tb close neighbours will give a contribution of the iron ferromagnetic component H_{hf}(Fe) = +(−)1.05(15) T and a contribution of the terbium sublattice H_{hf}(Tb) = −(+)1.00(8) T per Tb neighbour. The isotropic transfer constant of the iron ferromagnetic component to the hyperfine field will be $A_i = 1.05/6 \times 0.66 = 0.26\,T\,\mu_B{}^{-1}$ atom e^{-1}. This value is smaller than the values calculated with the data reported for the site 2(d) in $LFe_6Sn_4Ge_2$ (A_i = 0.56, 0.81, 0.53 T $\mu_B{}^{-1}$ atom e^{-1} for L = Tb, Dy, Ho respectively) [7,26].

It is more difficult to compare the contribution of the Tb sublattice with available data. However, it is worth noting that the uniaxial $HfFe_6Ge_6$-type $TbMn_6Sn_{5.8}Ga_{0.2}$ compound is characterized by a hyperfine field B_{hf} = 30.44 T on site 2(c) while the corresponding hyperfine field calculated for $HfFe_6Ge_6$-type $YMn_6Sn_{5.28}In_{0.72}$ compound in the same state is B_{hf} = 33.4 T [10,11]. This leads to $\Delta B_{hf} = -2.96$ T per 3 Tb nearest neighbours. In the same time, the reported hyperfine field on the 2(d) site with no Tb nearest neighbour changes from B_{hf} = 32.94 T in $TbMn_6Sn_{5.8}Ga_{0.2}$ to B_{hf} = 31.08 T in $YMn_6Sn_{5.28}In_{0.72}$. Scaling the 2(c) values for the same 2(d) values will give the enhanced difference $\Delta B_{hf} = -4.95$ T which enables the estimation of the Tb contribution in Mn-based compounds H_{hf}(Tb) ≈ 0.99 to1.65 T per Tb rather close to the value estimated for $TbFe_6Sn_6$.

Another interesting result deals with the variation of the amplitude of the transferred hyperfine fields at the low temperature magnetic transition (T_t = 27 K). The ordering of the Tb sublattice and the concomitant spin-reorientation of the AF component of the iron moments is associated, except for the Sn_5'' site, to a decrease of the amplitude of the hyperfine field of the Sn_5 subsites (Fig. 14). Since the transferred fields from the Tb moments and from the ferromagnetic Fe component will be directed along [1 0 0] and since the transferred field from the antiferromagnetic Fe component will be perpendicular to the [1 0 0] direction, we expect that the total hyperfine field on the Sn_{5i} nuclei will be proportional to the geometric sum of orthogonal vectors. Therefore, the reduction of the hyperfine field amplitude cannot account for a contribution of the Tb moments. We guess that this variation arises from the modification of the anisotropic contribution on the field transfer. The anisotropic contribution to the field transferred on the tin nucleus has been pointed out as the only way to explain the field transfer in the antiferromagnetic $FeSn_2$ compound [22]. Latter, this contribution has been also evidenced in manganese-based $LMn_6Sn_{6-x}M_x$ (M = Ga, In) compounds within which Mn spin-reorientations have been induced through the reorientation of the lanthanide moment or through the application of an external field on a pseudo-monocrystal sample [10,11]. This anisotropic contribution B_{ha} is given by the expression:

$$\vec{B}_{ha} = A_p \sum_{i=1}^{6} \vec{u}_i(\vec{\mu}_i \cdot \vec{u}_i) \tag{4}$$

where A_p is the anisotropic constant, $\vec{u}_i$ is the unit vector connecting each Sn atom to a specific Fe atom with moment $\vec{\mu}_i$. According to Eq. (4), the magnitude and direction of the anisotropic contribution depends on the relative direction between the moment and the corresponding T–Sn bonds. Its vectorial components derived from Eq. (4) are:

$$\vec{B}_{ha} = A_p \left\|\mu\right\| \begin{pmatrix} 6u_x^2 \cos\phi \\ 3u_y^2 \sin\phi \\ 0 \end{pmatrix}$$

where u_x and u_y are the components of the Fe–Sn unit bond vector as depicted in Fig. 15a and ϕ the angle between the Fe moment direction and the [1 0 0] axis. It may be observed that except for ϕ = 0 and 90°, the direction of the anisotropic field is not parallel to the Fe moment and, in turn, to the direction of the isotropic field. We can also note that, for the Sn_5'' atoms lying in the Fe plane (u_x = 0), there is no anisotropic contribution when μ_{Fe} is aligned along [1 0 0] whereas the anisotropic contribution is aligned along [0 1 0] when the Fe moment direction deviates from [1 0 0] ($\phi \neq 0°$). It is also worth noting that, due to the relative u_x and u_y values, the anisotropic field will be strongly enhanced when the angle ϕ value goes towards 90°. Therefore, the drastic reduction of the hyperfine field at the low temperature transition should be linked to opposite isotropic and anisotropic contributions. These situations are schematically depicted in Fig. 15b and c. The site Sn_5 displays a Tb atom as near neighbour and we have added the corresponding contribution at 4.2 K. The direction of the Tb transferred field has been deduced from the following angular considerations: (i) the angles between the isotropic and anisotropic contributions and the [1 0 0] axis are 73° and 87°, respectively (ii) from Eq. (3), the average Δ values at 4.2K and 32 K lead to a B_{hf} direction close to 78° from [1 0 0] (iii) to get this angle value from geometrical sum,

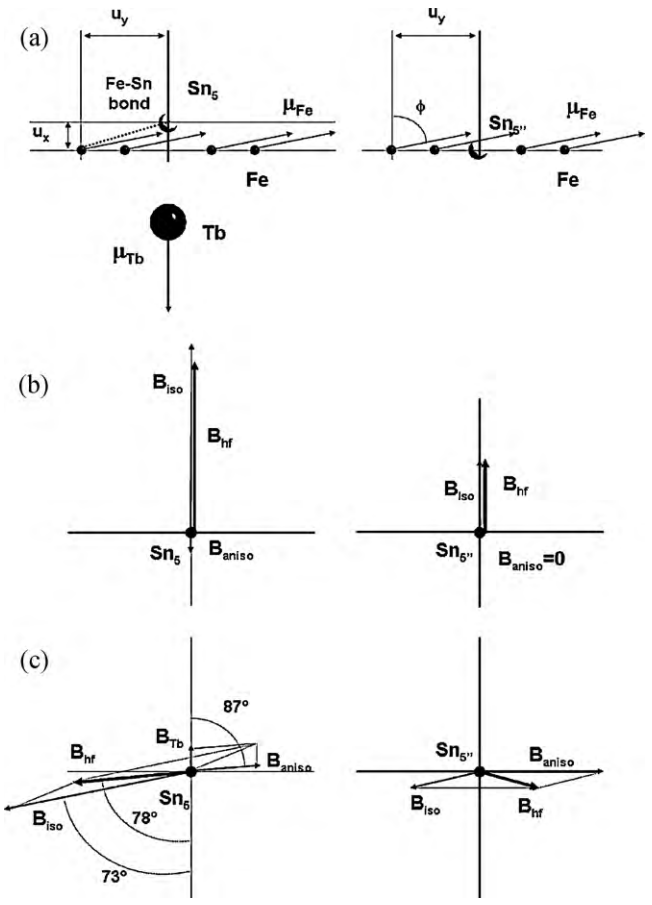

Fig. 15. (a) Environment of the Sn_5 and Sn_5'' sites and direction of the Fe–Sn bond with respect to the iron moment; (b) decomposition of the transferred hyperfine fields above 27 K; (c) decomposition of the transferred fields below 27 K.

the Tb contribution must be directed as depicted in Fig. 15c. With an iterative method, a rather good set of values is obtained: with B_{iso} = 24.9 T, B_{aniso} = 8.3 T and B_{Tb} = 3.3 T, angle value and magnitude of the hyperfine field are well reproduced. The value B_{Tb} may be compared to that estimated in $Gd_{1-x}Y_xMn_6Sn_6$ (B_{Gd} = 3.7 T) [27]. The case of Sn_5'' is slightly different since it has no Tb as near neighbour and the anisotropic contribution, aligned along [0 1 0], should be enhanced due to the orientation of the Fe–Sn bond. According to Fig. 15c, we can understand how the low temperature transition may be hidden for this site.

All these results may be compared to previous reports. In manganese-based compounds, it has been observed that the nearest are the moments and the Mn–Sn_{2e} bond directions, the strongest is the hyperfine field (for hexagonal $YMn_6Sn_{5.28}In_{0.72}$, ΔH = 6.4 T during the rotation towards the (0 0 1) plane [11]). This feature indicate that the anisotropic contribution is added to the isotropic contribution. In the present compound, it is observed that, when the Fe moment rotates towards the (1 0 0) plane, i.e. when the moment direction rotates towards the direction of the Fe–Sn_5 bond, the transferred hyperfine field suddenly decreases. Contrary to the manganese compounds, this peculiar behaviour rather indicates that the anisotropic and isotropic contributions have opposite signs. This feature might be related to band structure calculations performed on LMn_6Sn_6 and LFe_6Ge_6 compounds [24,25]. According to these studies, the computed Fermi contact hyperfine field values are strongly negative in Mn-based compounds and positive in iron germanides.

In the study of the LFe_6Ge_6 compounds, it is also pointed out the play of the partial filling of antibonding states. As the relative levels of bonding and antibonding states are connected to the corresponding interatomic distances, we wonder if the unusual hyperfine field values measured for the Sn_5' and Sn_5'' cannot also arise from this effect.

4. Conclusions

The study of $TbFe_6Sn_6$ displays an unusual magnetic behaviour of the two iron and terbium moments at the ordering point of the Tb sublattice. Since this behaviour might be the result of critical ratio of the various magnetic interactions, it might be interesting to check the properties of $Tb_{1-x}Fe_6Sn_6$ compounds with different terbium stoichiometries.

The spin-reorientation of the iron moments evidences an anisotropic contribution to the hyperfine field in a Fe-based compound. The relative isotropic and anisotropic contributions seem to be in good accordance with theoretical estimations.

Acknowledgement

We are indebted to the Institute Laue Langevin (Grenoble, France) for the provision of research facilities.

References

[1] Y.B. Wang, D. Wiarda, D.H. Ryan, J.M. Cadogan, IEEE Trans. Magn. 30 (6) (1994) 4951.
[2] D.H. Ryan, J.M. Cadogan, J. Appl. Phys. 79 (8 part 2B) (1996) 6004.
[3] X.L. Rao, M.D. Coey, J. Appl. Phys. 81 (8 part 2B) (1997) 5227.
[4] P. Schobinger-Papamantellos, O. Oleksyn, J. Rodriguez-Carvajal, G. André, E. Bruck, K.H.J. Buschow, J. Magn. Magn. Mater. 182 (1–2) (1998) 96.
[5] T. Mazet, B. Malaman, J. Magn. Magn. Mater. 219 (2000) 33.
[6] J.M. Cadogan, D.H. Ryan, J. Alloys Compd. 326 (2001) 166.
[7] K. Laura, D. Perry, H. Ryan, G. Venturini, B. Malaman, J. Alloys Compd. 436 (1–2) (2007) 1–8.
[8] G. Venturini, J. Alloys Compd. 400 (2005) 37.
[9] B. Chafik El Idrissi, G. Venturini, B. Malaman, Mater. Res. Bull. 26 (12) (1991) 1331–1338.
[10] K. Laura, D.H. Perry, G. Ryan, J.M. Venturini, Cadogan, J. Appl. Phys. 99 (2006), 08J302_1–08J302_3.
[11] K. Laura, D.H. Perry, G. Ryan, Venturini, Phys. Rev. B 75 (2007) 144417.
[12] B. Malaman, G. Venturini, J. Alloys Compd. 494 (1–2) (2010) 44.
[13] J. Rodriguez-Carvajal, Physica B 192 (1993) 55.
[14] G. le Caër, Private Communication.
[15] O. Nial, Z. Anorg. Allg. Chem. 238 (1938) 287.
[16] O. Oleksyn, H. Bohm, Z. Kristall. 213 (5) (1998) 270.
[17] O. Zaharko, P. Schobinger-Papamantellos, J. Rodriguez-Carvajal, K.H.J. Buschow, J. Alloys Compd. 288 (1–2) (1999) 50.
[18] J.M. Cadogan, D.H. Ryan, O. Moze, M. Suharyana, Hofmann, J. Phys.: Condens. Matter 15 (10) (2003) 1757–1771.
[19] J.M. Cadogan, D.H. Ryan, O. Moze, W. Kockelmann, IEEE Trans. Magn. 37 (4) (2001) 2606.
[20] P. Gaczynski, L.C.J. Pereira, J.C. Waerenborgh, J. Alloys Compd. 451 (2008) 484.
[21] P. Gaczynski, L.C.J. Pereira, J.C. Waerenborgh, J. Alloys Compd. 442 (2007) 158.
[22] G. Venturini, B. Malaman, G. Le Caër, D. Fruchart, Phys. Rev. B 35 (1987) 7038–7045.
[23] S.V. Karyagin, Fiz Tverd. Tela (Leningrad) 8 (1966) 493 (Sov. Phys.-Solid State (1966) 391).
[24] T. Mazet, J. Tobola, B. Malaman, Eur. Phys. J. B: Condens. Matter Phys. 33 (2) (2003) 183–191.
[25] T. Mazet, J. Tobola, G. Venturini, B. Malaman, Phys. Rev. B 65 (104406) (2002) 1–10.
[26] K. Laura, D. Perry, H. Ryan, G. Venturini, B. Malaman, J. Alloys Compd. 486 (2009) 29–36.
[27] G. Venturini, Private Communication, 2010.